Report

Current Biology

Dynamic Fluctuations in Subcellular Localization of the Hippo Pathway Effector Yorkie *In Vivo*

Highlights

- The key Hippo transcription coactivator Yorkie is enriched on mitotic chromatin
- Yorkie traffics dynamically between the nucleus and cytoplasm in interphase
- The rate of nuclear import of Yorkie varies substantially across growing organs
- The Hippo pathway kinase Warts limits the rate of nuclear import of Yorkie

Authors

Samuel A. Manning, Lucas G. Dent, Shu Kondo, Ziqing W. Zhao, Nicolas Plachta, Kieran F. Harvey

Correspondence

kieran.harvey@petermac.org

In Brief

Manning et al. investigate the subcellular dynamics of Yorkie, the key transcription regulator of the Hippo pathway, *in vivo*. They show that Yorkie is enriched on mitotic chromatin and that this depends on its DNA-binding partner, Scalloped. Yorkie nuclear import varies greatly across growing organs and is negatively regulated by the kinase Warts.

Manning et al., 2018, Current Biology *28*, 1651–1660
May 21, 2018
https://doi.org/10.1016/j.cub.2018.04.018

CellPress

Current Biology
Report

Dynamic Fluctuations in Subcellular Localization of the Hippo Pathway Effector Yorkie *In Vivo*

Samuel A. Manning,[1,2,3] Lucas G. Dent,[1,2] Shu Kondo,[4] Ziqing W. Zhao,[5] Nicolas Plachta,[5,6] and Kieran F. Harvey[1,2,3,7,*]
[1]Peter MacCallum Cancer Centre, 305 Grattan St., Melbourne, VIC 3000, Australia
[2]Sir Peter MacCallum Department of Oncology, University of Melbourne, Parkville, VIC 3010, Australia
[3]Department of Anatomy and Developmental Biology and Biomedicine Discovery Institute, Monash University, Clayton, VIC 3800, Australia
[4]Laboratory of Invertebrate Genetics, National Institute of Genetics, 1111 Yata, Mishima, Shizuoka 4118540, Japan
[5]Institute of Molecular and Cell Biology, Agency for Science, Technology and Research (A*STAR), Singapore 138632, Singapore
[6]Department of Biochemistry, Yong Loo Lin School of Medicine, National University of Singapore, Singapore 119228, Singapore
[7]Lead Contact
*Correspondence: kieran.harvey@petermac.org
https://doi.org/10.1016/j.cub.2018.04.018

SUMMARY

The Hippo pathway is an evolutionarily conserved signaling network that integrates diverse cues to control organ size and cell fate. The central downstream pathway protein in *Drosophila* is the transcriptional co-activator Yorkie (YAP and TAZ in humans), which regulates gene expression with the Scalloped/TEA domain family member (TEAD) transcription factors [1–8]. A central regulatory step in the Hippo pathway is phosphorylation of Yorkie by the NDR family kinase Warts, which promotes Yorkie cytoplasmic localization by stimulating association with 14-3-3 proteins [9–12]. Numerous reports have purported a static model of Hippo signaling whereby, upon Hippo activation, Yorkie/YAP/TAZ become cytoplasmic and therefore inactive, and upon Hippo repression, Yorkie/YAP/TAZ transit to the nucleus and are active. However, we have little appreciation for the dynamics of Yorkie/YAP/TAZ subcellular localization because most studies have been performed in fixed cells and tissues. To address this, we used live multiphoton microscopy to investigate the dynamics of an endogenously tagged Yorkie-Venus protein in growing epithelial organs. We found that the majority of Yorkie rapidly traffics between the cytoplasm and nucleus, rather than being statically localized in either compartment. In addition, discrete cell populations within the same organ display different rates of Yorkie nucleo-cytoplasmic shuttling. By assessing Yorkie dynamics in *warts* mutant tissue, we found that the Hippo pathway regulates Yorkie subcellular distribution by regulating its rate of nuclear import. Furthermore, Yorkie's localization fluctuates dramatically throughout the cell cycle, being predominantly cytoplasmic during interphase and, unexpectedly, chromatin enriched during mitosis. Yorkie's association with mitotic chromatin is Scalloped dependent, suggesting a potential role in mitotic bookmarking.

RESULTS AND DISCUSSION

Generation of *Drosophila* Expressing Endogenously Tagged Yorkie-Venus

Studies of Yorkie (Yki) subcellular localization in *D. melanogaster* and YAP and TAZ in mammals have focused primarily on fixed cells, using antibodies. Such studies are potentially limited because fixation can induce artifacts that can lead to errant conclusions [13]. Regulation of the localization of the Hippo pathway transcriptional co-activator protein Yki modulates its activity. As an approximation, Yki is thought to be nuclear when active and cytoplasmic when inactive. Surprisingly, in immunofluorescence-based studies of fixed growing organs, Yki appears to be predominantly cytoplasmic [9, 11, 14] (Figure 1A).

To investigate this key aspect of Hippo signaling using an alternate approach, we generated *D. melanogaster* that expressed an endogenously tagged Yki protein by inserting the coding sequence for Venus fluorescent protein into the 3′ end of the *yki* gene using CRISPR/Cas9 genome editing (Figure S1A). To verify this strain, we analyzed Yki-Venus expression by western blotting, which indicated the generation of fusion proteins of the expected molecular mass. Yki-Venus was slightly more abundant than endogenous Yki, indicating that the Venus tag may affect the stability of Yki protein or transcript (Figure S1B). Expression of a Yki RNAi transgene resulted in a strong reduction in both Yki and Venus proteins, further confirming successful creation of a Yki-Venus fusion protein (Figure S1C). Next, we compared the subcellular localization of Yki to Yki-Venus in fixed tissues. As previously described, Yki was broadly cytoplasmic in third instar larval wing and eye discs, and it was strongly expressed in cells surrounding photoreceptor clusters of eye discs (Figures S1D and S1F). These localization and expression patterns were shared by Yki-Venus (Figures 1A and S1E). Generation of homozygous *yki-venus* clones within a *yki* heterozygous background and subsequent staining for all forms of Yki using an antibody revealed similar subcellular distributions of Yki-Venus and Yki (Figure S1G). Overexpression of Scalloped (Sd) can promote nuclear accumulation of Yki [12, 15–17], and we observed the same phenomenon with Yki-Venus (Figure S1H). Finally, *yki-venus* flies were homozygous viable and fertile and exhibited no obvious developmental defects (Figure S1I), indicating that Yki-Venus is a functional protein. However, Yki

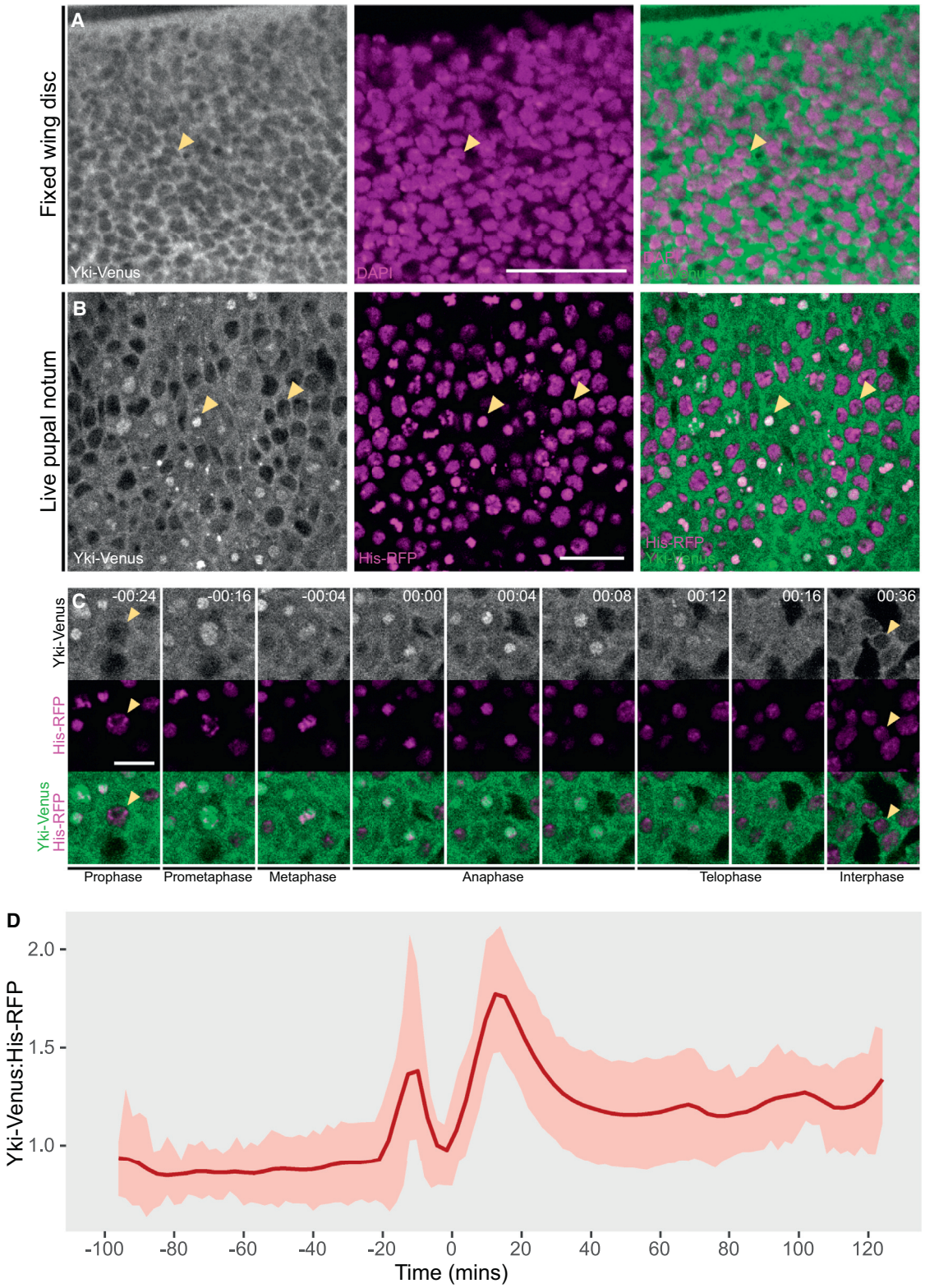

Figure 1. Live Imaging of Proliferating Organs Reveals Cell Cycle-Dependent Fluctuations in Yorkie Subcellular Localization

(A) Subcellular localization of Yki-Venus in fixed third instar larval wing imaginal discs, as revealed by a GFP antibody (grayscale and green). Chromatin is stained with DAPI (magenta). Yki appears to be predominantly cytoplasmic in all cells (example indicated by arrowhead).

(legend continued on next page)

function must be reduced partially as *yki-venus* hemizygous flies were lethal, possibly because of reduced interaction with its normal partners. In conclusion, while the Venus tag moderately affects Yki abundance, Yki-Venus is an accurate indicator of Yki subcellular localization.

Yki Colocalizes with Chromatin of Mitotic Epithelial Cells *In Vivo*

We next assessed the *in vivo* dynamics of Yki-Venus protein in the *D. melanogaster* pupal dorsal thorax, specifically, the notum and the scutellum. The notum is a monolayered epithelium that undergoes a period of growth following the prepupa-to-pupa transition [18], enabling imaging of tissue development in a non-invasive context. To enable demarcation of nuclei, chromatin was labeled with Histone2Av-monomeric red fluorescent protein (mRFP) (His-RFP) [19]. Time-lapse imaging was performed on fields of cells near the midline of the notum using z sections to capture the depth of the epithelium and allow tracking of chromatin as it moved apically and basally during mitosis. As previously reported in fixed larval imaginal discs using immunofluorescence, Yki-Venus was primarily cytoplasmic in most cells (Figure 1B). Strikingly, however, Yki-Venus displayed a strong association with chromatin of mitotic cells (Figure 1B; Video S1).

We quantified these dynamics by tracking cells as they progressed through mitosis, segmenting the chromatin and measuring the intensity of Yki-Venus. To normalize for changes in chromatin density that occur during mitosis and also for the halving of chromatin content at the point of chromatin separation, we calculated the ratio of Yki-Venus to His-RFP at each time point. We synchronized cells *in silico* to the frame of chromatin separation at the onset of anaphase to allow analysis of general trends. This revealed that the initial increase in colocalization of Yki-Venus and His-RFP was followed by a similarly rapid decrease as cells entered metaphase (Figures 1C and 1D; Video S1). This does not represent a total exclusion of Yki from chromatin as it was still clearly enriched on mitotic chromatin, compared to the cytoplasm. Following chromatin separation, there was a second spike in chromatin-localized Yki-Venus, which then gradually relocalized to the cytoplasm (Figure 1D). This was a general phenomenon, as similar results were observed in larval wing imaginal discs cultured *ex vivo* (Video S2).

We next re-examined Yki localization in fixed specimens by generating mosaic wing discs, containing patches of homozygous and heterozygous *yki-venus* and *yki* tissue, and staining these wing discs with antibodies against Yki and GFP. Interestingly, neither Yki nor Yki-Venus was detectable on mitotic chromatin using a Yki antibody (Figure S1J, second and right panels). Similar results were obtained with a GFP antibody in Yki-Venus-expressing tissue (Figure S1J, left panel). Therefore, tissue fixation must prevent the detection of chromatin-associated Yki in mitotic cells. This finding resembles a striking recent study that reported that multiple fluorescently tagged transcription factors were detected on mitotic chromatin by live imaging, but not in fixed tissues, because of a fixation artifact [20]. This overturned a long-standing dogma that most transcription factors are evicted from mitotic chromatin [20]. The observed association of Yki-Venus with mitotic chromatin is not a general feature of either fluorescent proteins or transcription factors, as neither yellow fluorescent protein (YFP) (98% identical to Venus) nor nuclear factor of activated T cells (NFAT)-GFP displayed enrichment on mitotic chromatin in pupal notum cells (Figures S2A and S2B). Finally, the cell cycle-dependent subcellular localization of Yki-Venus was not a result of it being slightly more abundant than wild-type Yki, because heterozygous *yki-venus* flies (which express similar amounts of Yki-Venus as wild-type flies express Yki) showed the same localization pattern throughout the cell cycle as *yki-venus* homozygotes (Figure 3A).

Yki Rapidly Exchanges between Mitotic Chromatin and the Cytoplasm

Next, we used fluorescence loss in photobleaching (FLIP) [21] to determine whether Yki associates with mitotic chromatin in a stable or dynamic manner. If Yki stably binds mitotic chromatin, bleaching the cytoplasm would not affect the chromatin-localized pool. However, if Yki exchanges between mitotic chromatin and the cytoplasm, bleaching the cytoplasm would decrease the chromatin-localized intensity as this pool turns over [22]. We conducted FLIP experiments on prophase cells by repeatedly bleaching a 1.25 × 1.25-μm region of the cytoplasm while imaging the whole cell. This bleaching and imaging cycle was repeated every 420 ms for approximately 2 min. Through repeated bleaching of the cytoplasm, we observed a rapid reduction of the chromatin-localized fraction of Yki-Venus (Figures 2A and 2B; Video S3, top left panel). By contrast, and as expected, His-RFP displayed stable chromatin localization throughout the imaging time course and only a low level of bleaching (data not shown). This indicates that the chromatin-localized fraction of Yki observed during prometaphase dynamically exchanges between the chromatin and cytoplasm.

(B) A single frame from a video acquired by multiphoton microscopic imaging of the notum of an early stage *D. melanogaster* pupa. The pupa expressed Yki-Venus (grayscale and green) and His-RFP, which marks chromatin (magenta). Yki is predominantly cytoplasmic in interphase cells but localized to chromatin in mitotic cells (examples of each are indicated by arrowheads). Scale bars, 20 μm.

(C) Images from single time points from a pupal notum similar to that captured in Video S1. The images are of Yki-Venus and His-RFP, allowing chromatin visualization and tracking throughout mitosis. Yki-Venus is in grayscale and in green in the merged images; His-RFP is magenta. Time is indicated in hr hr : min min relative to the approximate time of anaphase onset. Chromatin begins to condense during prophase (−00:24), and Yki-Venus colocalization with chromatin increases rapidly at prometaphase (−00:16). Chromatin separation occurs after metaphase (−00:04). Following anaphase, daughter chromatids segregate toward the poles (00:00) and chromatin-localized Yki-Venus continues to increase. As the daughter cells progress through telophase, the level of Yki-Venus localized with chromatin steadily decreases (00:08–00:36). Scale bar, 10 μm.

(D) A graph displaying the mean ratio of Yki-Venus:His-RFP intensities ± SD in 70 cells (140 daughter cells) from four pupae tracked during mitosis and synchronized *in silico* to the point of chromatin separation at anaphase (indicated by time 0 on the x axis). Two sharp peaks in chromatin localization of Yki-Venus are observed approximately 12 min prior to and following chromatin separation, roughly equating to prometaphase and the transition from anaphase to telophase, respectively.

See also Figures S1 and S2 and Videos S1 and S2.

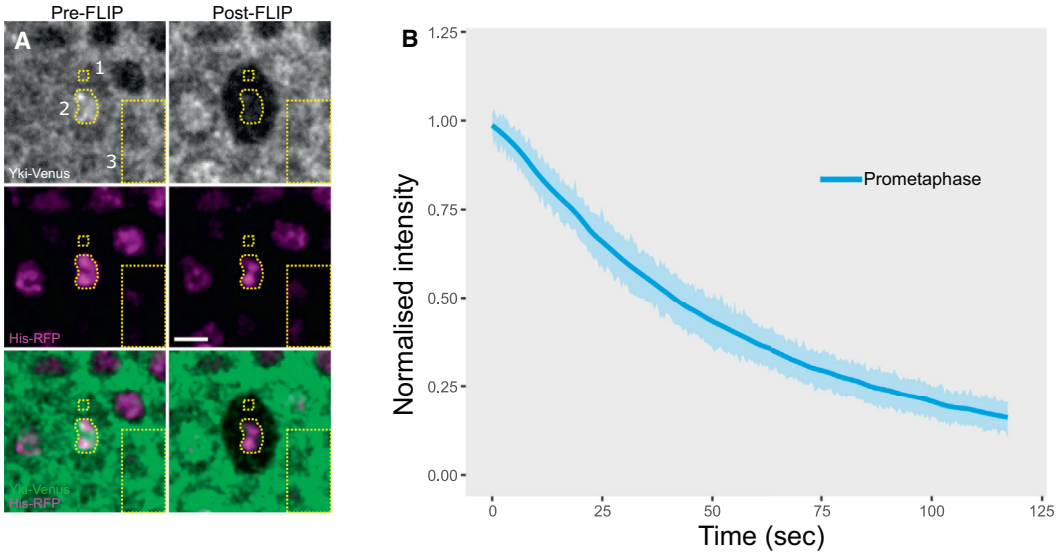

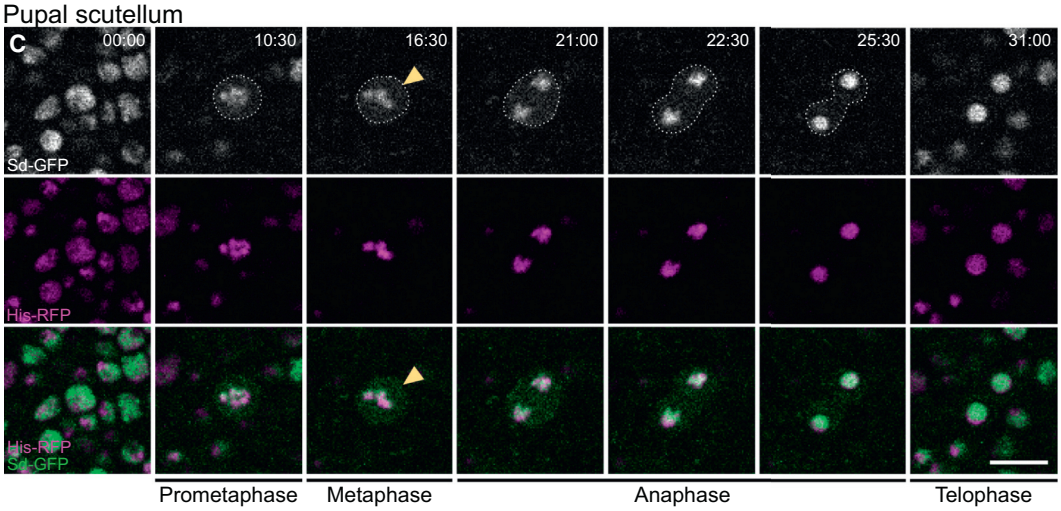

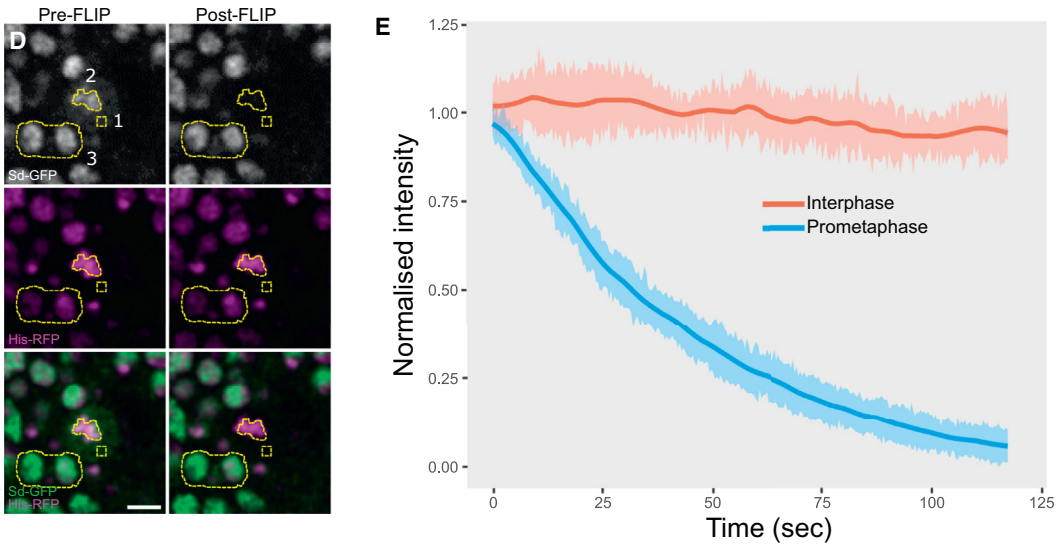

(legend on next page)

The Yki Partner, Sd, Exchanges between Chromatin and the Cytoplasm during Mitosis

We hypothesized that the relocalization of Yki-Venus at the onset of mitosis may correlate with the partial breakdown of the nuclear envelope that occurs during mitosis in *D. melanogaster*, resulting in a semi-open mitosis [23]. This could allow Yki unrestricted access to chromatin, where it may interact with binding partners such as the transcription factor Sd. In overexpression studies, Sd has been shown to enhance the localization of Yki to the nucleus [12, 15–17] (Figure S1H). As such, we investigated the localization of Sd throughout the cell cycle by live imaging a previously characterized *D. melanogaster* strain that expresses an Sd-GFP fusion protein [24–28]. Sd-GFP was expressed at low levels in the early pupal notum but at much higher levels in the scutellum, and so we performed imaging in the scutellum. In interphase cells, Sd-GFP localized very strongly to the nucleus (Figure 2C; Video S4). However, similar to Yki-Venus, Sd-GFP was dynamic during mitosis; as cells entered prometaphase, a distinct pool of Sd-GFP relocalized to the cytoplasm, evident as a diffuse halo around the chromatin (Figure 2C, arrowhead; Video S4). Notably, the majority of Sd-GFP remained colocalized with mitotic chromatin. Following chromatin separation at anaphase, the cytoplasmic pool of Sd-GFP very rapidly resolved to relocalize with chromatin (Figure 2C; Video S4). Similarly, Sd-GFP was predominantly chromatin localized throughout the cell cycle in third instar larval wing imaginal disc cells, with cytoplasmic Sd-GFP clearly evident during mitosis (data not shown).

We investigated whether Sd-GFP was stably associated with mitotic chromatin by performing FLIP analysis in prometaphase and metaphase cells in the pupal scutellum. Using the same repeated cytoplasmic bleaching and imaging protocol as for Yki-Venus, we observed a similarly rapid reduction in Sd-GFP signal when compared to the His-RFP signal from mitotic chromatin. This indicates that, like Yki-Venus, Sd-GFP is not stably associated with mitotic chromatin but exchanges rapidly between chromatin and the cytoplasm (Figures 2D and 2E; Video S3, bottom left panel). By contrast, similar experiments in interphase cells did not affect the chromatin-localized Sd-GFP pool, indicating that Sd does not appreciably transit between chromatin and the cytoplasm in interphase, at least not on the timescale studied here (Figure 2E; Video S3, bottom right panel).

Sd Promotes Localization of Yki to Chromatin during Mitosis

To further investigate possible functional interactions between Sd and Yki during mitosis, we analyzed the localization of Yki-Venus within the pupal notum in *sd* clones and neighboring *sd* heterozygous or wild-type tissue. We compared mean Yki-Venus intensity in the chromatin domain between *sd* cells and heterozygous or wild-type cells at different stages of mitosis, by drawing a region of interest (ROI) on the RFP channel and binning nuclei by cell cycle stage based on chromatin architecture. Both *sd* and control cells displayed a rapid increase in chromatin-localized Yki-Venus upon progression into prometaphase, as described above (Figures 3A and 3B, left panels). However, compared to control cells, *sd* cells displayed a reduction in chromatin-localized Yki-Venus, which was most evident at metaphase and anaphase (Figures 3A–3C). Sd expression varied substantially across many tissues, including the pupal thorax where it was more highly expressed in the scutellum than the notum (Figure S2C). The colocalization of Yki-Venus with mitotic chromatin between these two regions was indistinguishable, indicating that the relatively low levels of Sd in the notum are sufficient for Yki to localize to mitotic chromatin (Figure S2D). These data, along with the observation of Sd on mitotic chromatin, indicate that the strong localization of Yki to mitotic chromatin is mediated by Sd.

We also performed a quantitative analysis of Yki-Venus subcellular localization in *sd* cells that were in interphase. Overexpression of *sd* has been shown to enhance the nuclear localization of Yki in cell culture and *in vivo*, possibly through increased nuclear tethering. We sought to determine whether loss of Sd affects Yki shuttling, and so we blocked the nuclear export of Yki in *sd* mosaic wing discs with leptomycin B (LMB). At 80 min following LMB treatment, *sd* clones in the wing disc

Figure 2. Yorkie and Scalloped Rapidly Exchange between Chromatin and the Cytoplasm in Mitosis

(A) Images from single time points of a pupal notum captured in Video S3. FLIP was used to analyze the movement of chromatin-localized Yki-Venus between chromatin and the cytoplasm during prometaphase and metaphase. The pupa expressed Yki-Venus (grayscale in the signal image, green in the merged image) and His-RFP (magenta). Repeated bleaching of a cytoplasmic area (ROI 1) resulted in a rapid decrease in chromatin-localized intensity (ROI 2). ROI 3 marks the region used for neighbor cell normalization. Scale bar, 5 μm.

(B) A graph displaying mean Yki-Venus intensity within ROI 2 (chromatin) throughout the duration of FLIP experiments, as in Video S3. Data were background subtracted, corrected for acquisition photobleaching, and normalized to pre-bleach intensity. Trace displays mean values (n = 19 cells from two pupae) ± SD. See also Video S3.

(C) Images of single time points from time-lapse imaging of Sd-GFP and His-RFP in a pupal scutellum. Animals expressed Sd-GFP (grayscale in the signal image, green in the merged image) and His-RFP (magenta). Images are maximum-intensity projections of two z slices 1.5 μm apart. At the onset of prometaphase (10:30), a distinct pool of Sd-GFP relocalizes from chromatin to the cytoplasm (indicated by arrowheads), while some Sd-GFP remains localized to chromatin. The cytoplasmic Sd-GFP pool rapidly relocalizes to chromatin following chromatin separation after anaphase (from 21:00). Dashed lines demarcate cell outline when visible due to Sd-GFP distribution in the cytoplasm. Time elapsed from first frame is shown in min min :s s. Scale bar, 10 μm. See also Video S4.

(D) Images from single time points of a pupal scutellum captured in Video S3. FLIP was used to analyze the movement of chromatin-localized Sd-GFP between the chromatin and cytoplasm during prometaphase and metaphase. The pupa expressed Sd-GFP (grayscale in the signal image, green in the merged image) and His-RFP (magenta). Repeated bleaching of a cytoplasmic area (ROI 1) resulted in a rapid decrease in chromatin-localized intensity (ROI 2). ROI 3 marks the region used for neighbor cell normalization. Scale bar, 5 μm.

(E) A graph displaying mean Sd-GFP intensity within ROI 2 (chromatin) throughout the duration of FLIP experiments, as in Video S3. Blue trace indicates mean values for experiments using prometaphase/metaphase cells (n = 12 cells from three pupae), and red trace indicates mean values for experiments using interphase cells (n = 6 cells from three pupae) ± SD. Data were background subtracted, corrected for acquisition photobleaching, and normalized to pre-bleach intensity.

See also Video S3 and Figure S2.

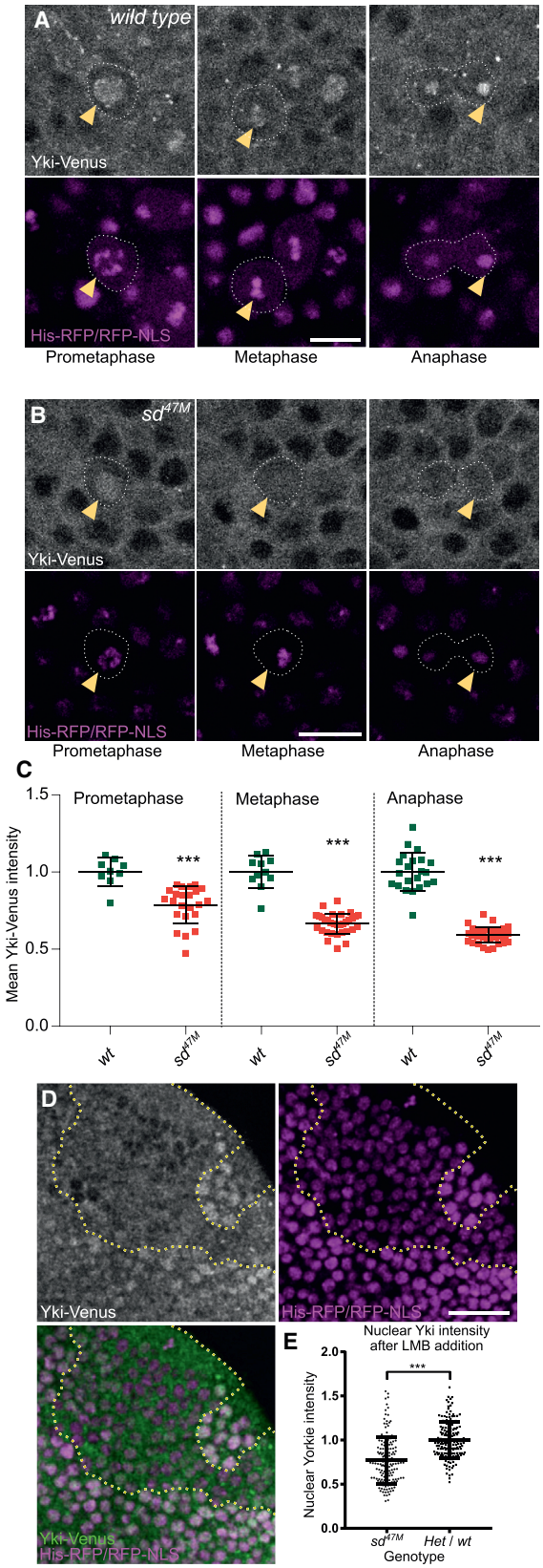

Figure 3. Scalloped Promotes Localization of Yorkie to Chromatin between Prometaphase and Anaphase

(A and B) Single-frame images from a video acquired by multiphoton microscopic imaging of a pupal notum harboring sd^{47M} clones. Yki-Venus is in grayscale and His-RFP and RFP-nls are in magenta. In (A) wild-type cells express RFP-nls (RFP signal distributed throughout the cell during mitosis), whereas in (B) sd^{47M} cells do not. Yki colocalizes with the chromatin of wild-type cells throughout mitosis, whereas in sd^{47M} mitotic cells it does not (examples are indicated by arrowheads). Approximate cell outlines are indicated by dashed white lines. Scale bars, 10 μm.

(C) A graph of chromatin-localized Yki-Venus in wild-type versus sd^{47M} tissue at the indicated stages of mitosis. In the sd^{47M} cells, the intensity of the Yki-Venus signal colocalizing with chromatin was significantly reduced at prometaphase, metaphase, and anaphase. Data represent the mean ± SD; ***p < 0.0001, unpaired t tests; prometaphase wild-type n = 9 cells, sd^{47M} n = 23 cells; metaphase wild-type n = 11 cells, sd^{47M} n = 32 cells; anaphase wild-type n = 22 cells, sd^{47M} n = 38 cells.

(D) Multiphoton image of an sd^{47M} mosaic live third instar wing imaginal disc notum expressing Yki-Venus (grayscale in top left panel, green in bottom left panel), which has been treated with LMB for 80 min. sd^{47M} tissue is marked by a reduced RFP signal (magenta) due to a lack of RFP-nls, and it is outlined with a dotted yellow line. Nuclei are marked by RFP-nls and His-RFP (magenta). Scale bar, 20 μm.

(E) Graph showing quantification of nuclear Yki-Venus intensity in sd^{47M} or heterozygous and wild-type tissue 80 min after LMB addition. Error bars show ± 1 SD; n = 156 cells (sd^{47M}) and 167 cells (heterozygous and wild-type) from 2 wing discs; ***p < 0.0001, two-tailed unpaired Student's t test.

See also Figure S2.

notum had reduced levels of nuclear Yki when compared to control cells, indicating that Sd promotes Yki nuclear accumulation (Figures 3D and 3E). The fact that chromosomal maintenance 1 (CRM1)-dependent nuclear export was blocked in this experiment implies that either less Yki was imported into the nucleus or that it could exit the nucleus of these cells, at least in part, in a CRM1-independent fashion, due to the loss of Sd-mediated retention. Finally, this observation bears some similarity to the finding that TEA domain family members (TEADs) promote TAZ nuclear localization in mammalian cultured cells [29].

Yki Rapidly Shuttles between the Nucleus and Cytoplasm during Interphase

Having observed the highly dynamic nature of Yki during mitosis, we next addressed Yki dynamics during interphase. Yki has been described as being mostly cytoplasmic in epithelial cells, which is thought to be due to cytoplasmic tethering of phosphorylated Yki by 14-3-3 proteins [9–12] and phosphorylation-independent junctional sequestration by Expanded [30]. Previous studies showed that long-term treatment of wing discs with LMB to block nuclear export leads to Yki nuclear accumulation [12, 31]. However, the timescale on which this translocation occurs has not been investigated. We hypothesized that, if most Yki is stably tethered in the cytoplasm, blocking nuclear export should have little effect on Yki localization in the short term. However, if Yki shuttles rapidly between the nucleus and the cytoplasm during interphase, blocking nuclear export should cause rapid accumulation of nuclear Yki and allow us to determine the rate at which nuclear import occurs. We therefore used live imaging to investigate the timescale of Yki nuclear translocation upon LMB treatment. Strikingly, within minutes of LMB treatment, Yki could be observed accumulating in nuclei (Figures 4A and 4B; Video S5).

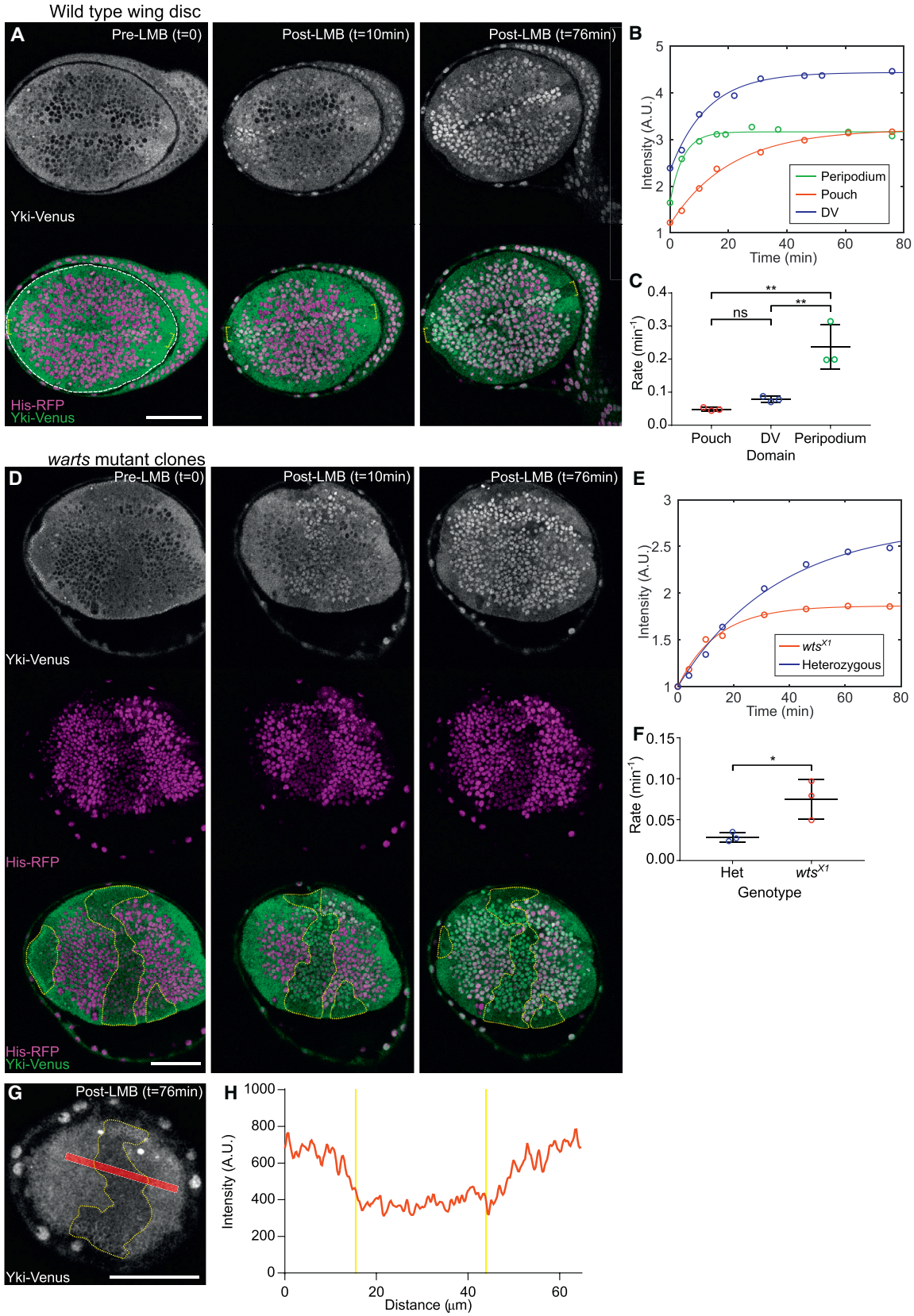

(legend on next page)

Yki's localization has been shown to be influenced both by nuclear import and export, although the relative contribution of these processes to the steady-state distribution of Yki has not been addressed. We observed variations in nuclear Yki-Venus intensity across the wing imaginal disc, with elevated nuclear levels along the dorsal-ventral boundary and in peripodial epithelial cells, when compared to cells within the wing pouch (Figure 4A, left panel, and Figure 4B, compare intensity at t = 0, before LMB addition). To address the contribution of nuclear import on Yki localization in these different cells, we compared the accumulation of Yki-Venus in response to LMB treatment. In each case, we normalized Yki-Venus intensity to the His-RFP signal. The rate of Yki nuclear accumulation in the peripodial membrane was between three and four times faster than cells within the pouch and the dorsoventral (DV) boundary (Figure 4C). Thus, the increased nuclear Yki in peripodial cells compared to pouch cells is due, at least in part, to increased rates of Yki nuclear import. Theoretically, this could result from different levels of Hippo signaling in these squamous epithelial cells, which has been proposed to be lower in these cells, compared to columnar epithelial cells of the disc proper [32]. The rates of Yki nuclear accumulation between the DV boundary and the pouch were not significantly different (Figure 4C), indicating that, in DV boundary cells, the increased nuclear abundance of Yki at steady state is likely to be caused by a decreased rate of nuclear export; a reduction in cytoplasmic sequestration; or an increase in some form of nuclear sequestration, either through binding to Sd or via an interaction with another nuclear sequestration factor, as hypothesized by Parker and Struhl [31]. While cytoplasmic tethering may contribute to the restriction of Yki from nuclei in interphase, our results indicate that Yki's cytoplasmic bias in interphase cells of the wing pouch is predominantly mediated by the rate of Yki nuclear export exceeding the rate of Yki nuclear import. Furthermore, these studies show that Yki's localization is not controlled by a static Hippo-on Hippo-off mechanism, as widely reported.

The Hippo Pathway Kinase Warts Regulates the Nuclear Import of Yki in Interphase

The Hippo pathway has been reported to control Yki's relative nuclear/cytoplasmic abundance by Warts (Wts)-mediated phosphorylation and subsequent association with 14-3-3 proteins [9–12]. In addition, Hippo has been shown to regulate the association of Yki with importins [17], but the relative contribution of Hippo-dependent nuclear import to the dynamics of Yki localization has not been addressed *in vivo*. Cells that lack the Yki kinase *wts* display increased levels of nuclear Yki, and we sought to address whether this was due to increased rates of nuclear import. Therefore, we cultured *wts* mosaic wing discs *ex vivo* with LMB, and we performed time-lapse imaging to compare the rate of nuclear accumulation of Yki-Venus in *wts* tissue compared to heterozygous tissue. The rate of nuclear accumulation of Yki-Venus in *wts* cells was approximately 2.5 times faster than in control cells (Figures 4D–4F; Video S6). This indicates that Wts regulates the nuclear localization of Yki predominantly by regulating its rate of nuclear import. Furthermore, at the endpoint of these experiments, when Yki nuclear accumulation had equilibrated across these mosaic tissues, we noticed residual cytoplasmic Yki in wild-type, but not *wts*, cells (Figures 4G and 4H). This was most evident in non-nuclear planes of these tissues, showing that Wts impedes a minor pool of Yki from shuttling between the nucleus and cytoplasm during interphase. Wts does not generally affect transcription factor localization, as a GFP-tagged version of Mastermind was similarly localized in both *wts* and wild-type cells (Figure S2E).

Conclusions

Here, using live multiphoton microscopy of growing epithelial organs, we find that the key transcription regulator Yki dynamically transits between the nucleus and cytoplasm and that the Hippo pathway regulates Yki nucleo-cytoplasmic shuttling by regulating its rate of nuclear import. Further, discrete cell populations within the same organ can display different Yki nucleo-cytoplasmic ratios, and these can be dictated by the

Figure 4. The Hippo Pathway Regulates the Rate of Nuclear Import of Yorkie

(A) Images from single time points (before and 10 and 76 min after drug addition) from time-lapse imaging of live wing imaginal discs cultured *ex vivo* in the presence of LMB. Yki-Venus is grayscale in single-panel images and green in the merged images; His-RFP is magenta. The wing pouch is outlined with a white dashed line in the lower left panel. The dorsal-ventral boundary is marked by yellow dashed brackets in merged panels. Scale bar, 50 μm. See also Video S5.

(B) A graph of nuclear intensity of Yki-Venus normalized to His-RFP for the three indicated regions of the wing imaginal disc at multiple time points after the addition of LMB.

(C) A graph of extracted rate constants of nuclear accumulation of Yki-Venus in the pouch, dorsal-ventral boundary, and the peripodial epithelium. ns, not significant ($p > 0.05$); **$p < 0.01$, one-way ANOVA with Tukey's multiple comparison test.

(D) Images from single time points (before and 10 and 76 min after drug addition) from time-lapse imaging of live wing imaginal discs containing wts^{X1} mutant clones (outlined with dotted yellow lines) cultured *ex vivo* in the presence of LMB. Yki-Venus is grayscale in single-panel images and green in the merged images, and His-RFP and RFP-nls are magenta. His-RFP marks chromatin in all cells, while RFP-nls is only expressed in heterozygous and homozygous wild-type cells. As such, the RFP signal is lower in *wts* mutant cells. Scale bar, 50 μm. See also Video S6 and Figure S2.

(E) A graph of nuclear intensity of Yki-Venus normalized to RFP in both heterozygous and wts^{X1} mutant cells at multiple time points after the addition of LMB. Values are normalized to pre-LMB addition (t = 0).

(F) A graph of extracted rate constants of the nuclear accumulation of Yki-Venus in wts^{X1} heterozygous and homozygous cells from three independent wing discs. *$p < 0.05$, two-tailed unpaired Student's t test. Points plotted in (B) and (E) represent the mean of three repeats, and the lines represent a best fit of the mean of these data using the equation described in the text. In each repeat, at least 30 cells were measured in each domain or for each genotype at each time point, and nuclei were manually outlined using a uniform circular ROI based on the RFP channel. The rate constants in (C) and (F) were extracted from individual fits of each repeat and are plotted with mean ± 1 SD.

(G) Yki-Venus (grayscale) in an apical section of the same wing disc shown in (D) 76 min after LMB addition. Yellow dotted line outlines the wts^{X1} mutant clone. Red line indicates the region used for intensity line plot in (H). Image was treated with Gaussian blur for analysis (σ = 1 pixel) and line width was 15 pixels. Scale bar, 50 μm.

(H) Intensity line plot of 15-pixel-wide red line shown in (G), with distance along line from left to right of (G) plotted on the x axis. Yellow vertical lines indicate approximate wts^{X1} clone boundaries.

modulation of either Yki nuclear import or export. Similarly, the nucleo-cytoplasmic distribution of YAP and TAZ, the mammalian orthologs of Yki, can be influenced by both nuclear import and export in cultured cells [29, 33]. Intriguingly, the subcellular localization of Yki fluctuates throughout the cell cycle; Yki is predominantly cytoplasmic throughout the majority of the cell cycle, but it is enriched on the chromatin of mitotic cells.

At first glance, it seems paradoxical that a transcription regulator would accumulate on chromatin during mitosis, when chromatin compacts and transcription largely ceases, although there are increasing reports for this [20, 34, 35]. Two possible mitotic roles for Yki are clearance of paused RNA polymerase II prior to metaphase and mitotic bookmarking. Elongation of paused RNA polymerase II occurs during mitosis [36], and YAP and TAZ associate with transcription elongation factors such as Cdk9 and promote elongation [37]. This has not been examined in *Drosophila*, but, given the high degree of conservation inherent in the Hippo pathway, it is plausible that Yki could also promote transcription elongation. Mitotic bookmarking involves recruitment and/or retention of transcription factors during mitosis to activate transcription immediately following cytokinesis [38, 39]. This was initially thought to be a property of only select transcription factors, although is now known to be far more common [20, 34, 35]. Yki and Sd have been linked to regulation of many essential genes, such as those involved in cell survival and metabolism [40, 41]. If Yki and Sd engage in mitotic bookmarking, they might promote the expression of such genes immediately following cytokinesis to ensure cell viability.

STAR★METHODS

Detailed methods are provided in the online version of this paper and include the following:

- KEY RESOURCES TABLE
- CONTACT FOR REAGENT AND RESOURCE SHARING
- EXPERIMENTAL MODEL AND SUBJECT DETAILS
- METHOD DETAILS
  - *D. melanogaster* strains
  - Generation of the Yki-venus strain
  - Immunofluorescence
  - Immunoblotting
  - *In vivo* imaging of *D. melanogaster* pupae
  - Quantification of time-lapse analysis of Yki-Venus
  - *Ex vivo* culture of wing imaginal discs
  - Treatment of imaginal discs with leptomycin B
  - Quantification of nuclear accumulation rates
  - Fluorescence loss in photobleaching
  - Quantification of mitotic Yki-Venus
- QUANTIFICATION AND STATISTICAL ANALYSIS

SUPPLEMENTAL INFORMATION

Supplemental Information includes two figures and six videos and can be found with this article online at https://doi.org/10.1016/j.cub.2018.04.018.

ACKNOWLEDGMENTS

We thank Nicolas Tapon for discussions, Yanina Alvarez for assistance with data analysis, and the Peter Mac Microscopy and Histology Core facility for assistance. We thank Jin Jiang, Iswar Hariharan, Duojia Pan, Nicolas Tapon, the Vienna *Drosophila* Resource Center, the Australian *Drosophila* Research Support Facility (http://www.ozdros.com), the Bloomington *Drosophila* Stock Center, and the Developmental Studies Hybridoma Bank for *D. melanogaster* stocks and antibodies. K.F.H. is a National Health and Medical Research Council Senior Research Fellow. S.A.M. was supported by an Australian Postgraduate Award. This research was supported by the National Health and Medical Research Council of Australia (1078220 and 1080131) and the CASS Foundation.

AUTHOR CONTRIBUTIONS

Conceptualization, S.A.M. and K.F.H.; Methodology, S.A.M.; Investigation, S.A.M. and L.G.D.; Formal Analysis, S.A.M., L.G.D., Z.W.Z., and N.P.; Writing—Original Draft, S.A.M., L.G.D., and K.F.H.; Resources, S.K.; Supervision, K.F.H.; Funding Acquisition, K.F.H.

DECLARATION OF INTERESTS

The authors declare no competing interests.

Received: March 5, 2018
Revised: April 4, 2018
Accepted: April 5, 2018
Published: May 10, 2018

REFERENCES

1. Gaspar, P., and Tapon, N. (2014). Sensing the local environment: actin architecture and Hippo signalling. Curr. Opin. Cell Biol. *31*, 74–83.
2. Zhao, B., Tumaneng, K., and Guan, K.L. (2011). The Hippo pathway in organ size control, tissue regeneration and stem cell self-renewal. Nat. Cell Biol. *13*, 877–883.
3. Halder, G., and Johnson, R.L. (2011). Hippo signaling: growth control and beyond. Development *138*, 9–22.
4. Pan, D. (2010). The hippo signaling pathway in development and cancer. Dev. Cell *19*, 491–505.
5. Enderle, L., and McNeill, H. (2013). Hippo gains weight: added insights and complexity to pathway control. Sci. Signal. *6*, re7.
6. Irvine, K.D., and Harvey, K.F. (2015). Control of organ growth by patterning and hippo signaling in Drosophila. Cold Spring Harb. Perspect. Biol. *7*, a019224.
7. Barry, E.R., and Camargo, F.D. (2013). The Hippo superhighway: signaling crossroads converging on the Hippo/Yap pathway in stem cells and development. Curr. Opin. Cell Biol. *25*, 247–253.
8. Halder, G., Dupont, S., and Piccolo, S. (2012). Transduction of mechanical and cytoskeletal cues by YAP and TAZ. Nat. Rev. Mol. Cell Biol. *13*, 591–600.
9. Oh, H., and Irvine, K.D. (2008). In vivo regulation of Yorkie phosphorylation and localization. Development *135*, 1081–1088.
10. Zhao, B., Wei, X., Li, W., Udan, R.S., Yang, Q., Kim, J., Xie, J., Ikenoue, T., Yu, J., Li, L., et al. (2007). Inactivation of YAP oncoprotein by the Hippo pathway is involved in cell contact inhibition and tissue growth control. Genes Dev. *21*, 2747–2761.
11. Dong, J., Feldmann, G., Huang, J., Wu, S., Zhang, N., Comerford, S.A., Gayyed, M.F., Anders, R.A., Maitra, A., and Pan, D. (2007). Elucidation of a universal size-control mechanism in Drosophila and mammals. Cell *130*, 1120–1133.
12. Ren, F., Zhang, L., and Jiang, J. (2010). Hippo signaling regulates Yorkie nuclear localization and activity through 14-3-3 dependent and independent mechanisms. Dev. Biol. *337*, 303–312.
13. Schnell, U., Dijk, F., Sjollema, K.A., and Giepmans, B.N. (2012). Immunolabeling artifacts and the need for live-cell imaging. Nat. Methods *9*, 152–158.
14. Poon, C.L., Zhang, X., Lin, J.I., Manning, S.A., and Harvey, K.F. (2012). Homeodomain-interacting protein kinase regulates Hippo pathway-dependent tissue growth. Curr. Biol. *22*, 1587–1594.

15. Zhang, L., Ren, F., Zhang, Q., Chen, Y., Wang, B., and Jiang, J. (2008). The TEAD/TEF family of transcription factor Scalloped mediates Hippo signaling in organ size control. Dev. Cell *14*, 377–387.
16. Goulev, Y., Fauny, J.D., Gonzalez-Marti, B., Flagiello, D., Silber, J., and Zider, A. (2008). SCALLOPED interacts with YORKIE, the nuclear effector of the hippo tumor-suppressor pathway in Drosophila. Curr. Biol. *18*, 435–441.
17. Wang, S., Lu, Y., Yin, M.X., Wang, C., Wu, W., Li, J., Wu, W., Ge, L., Hu, L., Zhao, Y., and Zhang, L. (2016). Importin α1 Mediates Yorkie Nuclear Import via an N-terminal Non-canonical Nuclear Localization Signal. J. Biol. Chem. *291*, 7926–7937.
18. Bosveld, F., Bonnet, I., Guirao, B., Tlili, S., Wang, Z., Petitalot, A., Marchand, R., Bardet, P.L., Marcq, P., Graner, F., and Bellaïche, Y. (2012). Mechanical control of morphogenesis by Fat/Dachsous/Four-jointed planar cell polarity pathway. Science *336*, 724–727.
19. Schuh, M., Lehner, C.F., and Heidmann, S. (2007). Incorporation of Drosophila CID/CENP-A and CENP-C into centromeres during early embryonic anaphase. Curr. Biol. *17*, 237–243.
20. Teves, S.S., An, L., Hansen, A.S., Xie, L., Darzacq, X., and Tjian, R. (2016). A dynamic mode of mitotic bookmarking by transcription factors. eLife *5*, e22280.
21. Nissim-Rafinia, M., and Meshorer, E. (2011). Photobleaching assays (FRAP & FLIP) to measure chromatin protein dynamics in living embryonic stem cells. J. Vis. Exp. (52), 2696.
22. Köster, M., Frahm, T., and Hauser, H. (2005). Nucleocytoplasmic shuttling revealed by FRAP and FLIP technologies. Curr. Opin. Biotechnol. *16*, 28–34.
23. Stafstrom, J.P., and Staehelin, L.A. (1984). Dynamics of the nuclear envelope and of nuclear pore complexes during mitosis in the Drosophila embryo. Eur. J. Cell Biol. *34*, 179–189.
24. Neto-Silva, R.M., de Beco, S., and Johnston, L.A. (2010). Evidence for a growth-stabilizing regulatory feedback mechanism between Myc and Yorkie, the Drosophila homolog of Yap. Dev. Cell *19*, 507–520.
25. Pastor-Pareja, J.C., and Xu, T. (2011). Shaping cells and organs in Drosophila by opposing roles of fat body-secreted Collagen IV and perlecan. Dev. Cell *21*, 245–256.
26. Corty, M.M., Tam, J., and Grueber, W.B. (2016). Dendritic diversification through transcription factor-mediated suppression of alternative morphologies. Development *143*, 1351–1362.
27. Buszczak, M., Paterno, S., Lighthouse, D., Bachman, J., Planck, J., Owen, S., Skora, A.D., Nystul, T.G., Ohlstein, B., Allen, A., et al. (2007). The carnegie protein trap library: a versatile tool for Drosophila developmental studies. Genetics *175*, 1505–1531.
28. Koontz, L.M., Liu-Chittenden, Y., Yin, F., Zheng, Y., Yu, J., Huang, B., Chen, Q., Wu, S., and Pan, D. (2013). The Hippo effector Yorkie controls normal tissue growth by antagonizing scalloped-mediated default repression. Dev. Cell *25*, 388–401.
29. Chan, S.W., Lim, C.J., Loo, L.S., Chong, Y.F., Huang, C., and Hong, W. (2009). TEADs mediate nuclear retention of TAZ to promote oncogenic transformation. J. Biol. Chem. *284*, 14347–14358.
30. Badouel, C., Gardano, L., Amin, N., Garg, A., Rosenfeld, R., Le Bihan, T., and McNeill, H. (2009). The FERM-domain protein Expanded regulates Hippo pathway activity via direct interactions with the transcriptional activator Yorkie. Dev. Cell *16*, 411–420.
31. Parker, J., and Struhl, G. (2015). Scaling the Drosophila Wing: TOR-Dependent Target Gene Access by the Hippo Pathway Transducer Yorkie. PLoS Biol. *13*, e1002274.
32. Fletcher, G.C., Diaz-de-la-Loza, M.D., Borreguero-Muñoz, N., Holder, M., Aguilar-Aragon, M., and Thompson, B.J. (2018). Mechanical strain regulates the Hippo pathway in *Drosophila*. Development *145*, dev159467.
33. Elosegui-Artola, A., Andreu, I., Beedle, A.E.M., Lezamiz, A., Uroz, M., Kosmalska, A.J., Oria, R., Kechagia, J.Z., Rico-Lastres, P., Le Roux, A.L., et al. (2017). Force Triggers YAP Nuclear Entry by Regulating Transport across Nuclear Pores. Cell *171*, 1397–1410.e14.
34. Lodhi, N., Ji, Y., and Tulin, A. (2016). Mitotic bookmarking: maintaining post-mitotic reprogramming of transcription reactivation. Curr. Mol. Biol. Rep. *2*, 10–16.
35. Hsiung, C.C., Morrissey, C.S., Udugama, M., Frank, C.L., Keller, C.A., Baek, S., Giardine, B., Crawford, G.E., Sung, M.H., Hardison, R.C., and Blobel, G.A. (2015). Genome accessibility is widely preserved and locally modulated during mitosis. Genome Res. *25*, 213–225.
36. Liang, K., Woodfin, A.R., Slaughter, B.D., Unruh, J.R., Box, A.C., Rickels, R.A., Gao, X., Haug, J.S., Jaspersen, S.L., and Shilatifard, A. (2015). Mitotic Transcriptional Activation: Clearance of Actively Engaged Pol II via Transcriptional Elongation Control in Mitosis. Mol. Cell *60*, 435–445.
37. Galli, G.G., Carrara, M., Yuan, W.C., Valdes-Quezada, C., Gurung, B., Pepe-Mooney, B., Zhang, T., Geeven, G., Gray, N.S., de Laat, W., et al. (2015). YAP Drives Growth by Controlling Transcriptional Pause Release from Dynamic Enhancers. Mol. Cell *60*, 328–337.
38. John, S., and Workman, J.L. (1998). Bookmarking genes for activation in condensed mitotic chromosomes. BioEssays *20*, 275–279.
39. Michelotti, E.F., Sanford, S., and Levens, D. (1997). Marking of active genes on mitotic chromosomes. Nature *388*, 895–899.
40. Oh, H., Slattery, M., Ma, L., Crofts, A., White, K.P., Mann, R.S., and Irvine, K.D. (2013). Genome-wide association of Yorkie with chromatin and chromatin-remodeling complexes. Cell Rep. *3*, 309–318.
41. Slattery, M., Voutev, R., Ma, L., Nègre, N., White, K.P., and Mann, R.S. (2013). Divergent transcriptional regulatory logic at the intersection of tissue growth and developmental patterning. PLoS Genet. *9*, e1003753.
42. Emery, G., Hutterer, A., Berdnik, D., Mayer, B., Wirtz-Peitz, F., Gaitan, M.G., and Knoblich, J.A. (2005). Asymmetric Rab 11 endosomes regulate delta recycling and specify cell fate in the Drosophila nervous system. Cell *122*, 763–773.
43. Schindelin, J., Arganda-Carreras, I., Frise, E., Kaynig, V., Longair, M., Pietzsch, T., Preibisch, S., Rueden, C., Saalfeld, S., Schmid, B., et al. (2012). Fiji: an open-source platform for biological-image analysis. Nat. Methods *9*, 676–682.
44. Tinevez, J.Y., Perry, N., Schindelin, J., Hoopes, G.M., Reynolds, G.D., Laplantine, E., Bednarek, S.Y., Shorte, S.L., and Eliceiri, K.W. (2017). TrackMate: An open and extensible platform for single-particle tracking. Methods *115*, 80–90.
45. de Chaumont, F., Dallongeville, S., Chenouard, N., Hervé, N., Pop, S., Provoost, T., Meas-Yedid, V., Pankajakshan, P., Lecomte, T., Le Montagner, Y., et al. (2012). Icy: an open bioimage informatics platform for extended reproducible research. Nat. Methods *9*, 690–696.
46. Vissers, J.H., Manning, S.A., Kulkarni, A., and Harvey, K.F. (2016). A Drosophila RNAi library modulates Hippo pathway-dependent tissue growth. Nat. Commun. *7*, 10368.
47. Xue, Z., Ren, M., Wu, M., Dai, J., Rong, Y.S., and Gao, G. (2014). Efficient gene knock-out and knock-in with transgenic Cas9 in Drosophila. G3 (Bethesda) *4*, 925–929.
48. Poon, C.L., Mitchell, K.A., Kondo, S., Cheng, L.Y., and Harvey, K.F. (2016). The Hippo Pathway Regulates Neuroblasts and Brain Size in Drosophila melanogaster. Curr. Biol. *26*, 1034–1042.
49. Horn, C., Jaunich, B., and Wimmer, E.A. (2000). Highly sensitive, fluorescent transformation marker for Drosophila transgenesis. Dev. Genes Evol. *210*, 623–629.
50. Kondo, S., and Ueda, R. (2013). Highly improved gene targeting by germline-specific Cas9 expression in Drosophila. Genetics *195*, 715–721.
51. Zitserman, D., and Roegiers, F. (2011). Live-cell imaging of sensory organ precursor cells in intact Drosophila pupae. J. Vis. Exp. (51), 2706.

STAR★METHODS

KEY RESOURCES TABLE

REAGENT or RESOURCE	SOURCE	IDENTIFIER
Antibodies		
Chicken polyclonal anti-GFP	Abcam	Cat#ab13970; RRID:AB_300798
Guinea pig polyclonal anti-Yki	Iswar Hariharan	N/A
Mouse monoclonal anti-Tubulin	DSHB	Cat#E7; RRID:AB_528499
Mouse monoclonal anti-rat CD2	AbD Serotec	Cat#MCA154GA; RRID:AB_566608
Goat anti-chicken 488	Life technologies	Cat#A11039; RRID:AB_142924
Donkey anti-mouse 555	Thermo Fisher Scientific	Cat#A31570; RRID:AB_2536180
Goat anti-guinea pig 647	Invitrogen Molecular Probes	A21450; RRID:AB_141882
Chemicals, Peptides, and Recombinant Proteins		
Leptomycin B solution from Streptomyces sp.	Sigma-Aldrich	L2913; CAS:87081-35-4
Insulin solution from bovine pancreas	Sigma-Aldrich	I0516
Experimental Models: Organisms/Strains		
D. melanogaster: Yki-Venus: w; Yki-Venus	This paper	N/A
D. melanogaster: His-RFP: w[*]; P{w[+mC] = His2Av-mRFP1}II.2	Bloomington Drosophila Stock Centre	BDSC:23651; FlyBase:FBst0023651; RRID:BDSC_23651
D. melanogaster: Sd-GFP: y[1] w[*] P{w[+mC] = PTT-GA}sd[CA07575]	Bloomington Drosophila Stock Centre	BDSC:50827; FlyBase:FBst0050827; RRID:BDSC_50827
D. melanogaster: w1118: w[1118]	Bloomington Drosophila Stock Centre	BDSC:3605; FlyBase:FBst0003605
D. melanogaster: actin flip-out	Bloomington Drosophila Stock Centre	BDSC:4780; FlyBase:FBst0004780; RRID:BDSC_4780
D. melanogaster: RNAi of Yki: P{KK104523}VIE-260B	Vienna Drosophila Resource Center	VDRC:104523; RRID:FlyBase_FBst0479676
D. melanogaster: UAS-His-RFP	Helena Richardson [42]	N/A
D. melanogaster: UAS-Sd: w[*]; P{w[+mC] = UAS-sd.S}V1	Bloomington Drosophila Stock Centre	BDSC:9373; FlyBase:FBst0009373; RRID:BDSC_9373
D. melanogaster: FRT19A scalloped47M	Duojia Pan	N/A
D. melanogaster: FRT19A RFP-nls hsFLP: P{w[+mC] = Ubi-mRFP.nls}1, w[*], P{ry[+t7.2] = hsFLP}12 P{ry[+t7.2] = neoFRT}19A	Bloomington Drosophila Stock Centre	BDSC:31418; FlyBase:FBst0031418; RRID:BDSC_31418
D. melanogaster: FRT82B wartsX1: w[*]; wts[x1] P{ry[+t7.2] = neoFRT}82B/TM6B, Tb [1]	Bloomington Drosophila Stock Centre	BDSC:44251; FlyBase:FBst0044251; RRID:BDSC_44251
D. melanogaster: FRT82B RFP-nls: w[1118]; P{ry[+t7.2] = neoFRT}82B P{w[+mC] = Ubi-mRFP.nls}3R	Bloomington Drosophila Stock Centre	BDSC:30555; FlyBase:FBst0030555; RRID:BDSC_30555
D. melanogaster: FRT42D RFP-nls: y[1] w[1118]; P{ry[+t7.2] = neoFRT}42D P{w[+mC] = Ubi-mRFP.nls}2R	Bloomington Drosophila Stock Centre	BDSC:35496; FlyBase:FBst0035496; RRID:BDSC_35496
D. melanogaster: Pannier-Gal4 (UAS-Dcr removed): P{w[+mC] = UAS-Dcr-2.D}1, w[1118]; P{w[+mW.hs] = GawB}pnr[MD237]/TM3, Ser [1]	Bloomington Drosophila Stock Centre	BDSC:25758; FlyBase:FBst0025758; RRID:BDSC_25758
D. melanogaster: UAS-YFP: y[*] w[*]; P{w[+mC] = UAS-2xEYFP}AH2	Bloomington Drosophila Stock Centre	BDSC:6659; FlyBase:FBst0006659; RRID:BDSC_6659
D. melanogaster: NFAT-GFP: y[1] w[*] P{w[+mC] = PTT-GA}NFAT[CA07788]	Bloomington Drosophila Stock Centre	BDSC:50832; FlyBase:FBst0050832; RRID:BDSC_50832
D. melanogaster: mastermind-GFP: y[1] w[67c23]; Mi{PT-GFSTF.0}mam[MI03814-GFSTF.0]/CyO	Bloomington Drosophila Stock Centre	BDSC:59812; FlyBase:FBst0059812; RRID:BDSC_59812

(*Continued on next page*)

Continued		
REAGENT or RESOURCE	SOURCE	IDENTIFIER
Software and Algorithms		
MATLAB R2017b	The MathWorks	https://www.mathworks.com/products/matlab.html
GraphPad Prism 7	GraphPad Software	https://www.graphpad.com/scientific-software/prism/
FIJI	[43]	https://fiji.sc/
TrackMate	[44]	https://imagej.net/TrackMate
Icy	[45]	http://icy.bioimageanalysis.org/
Other		
Grace Bio-Labs CoverWell perfusion chambers	Sigma-Aldrich	Cat#GBL622503

CONTACT FOR REAGENT AND RESOURCE SHARING

Further information and requests for resources and reagents should be directed to and will be fulfilled by the Lead Contact, Kieran F. Harvey (kieran.harvey@petermac.org)

EXPERIMENTAL MODEL AND SUBJECT DETAILS

Drosophila melanogaster stocks were maintained on standard medium at room temperature (22°C) and experimental crosses were carried out at 25°C.

METHOD DETAILS

D. melanogaster strains

w1118
yki-venus His2Av-mRFP / yki-venus
y w hsFLP; FRT42D Ubi-RFP-nls / FRT42D yki-venus
y w hsFLP; yki-venus / UAS-yki RNAi; act > CD2 > GAL4 UAS-His-RFP (the *yki* KK RNAi line was recombined to remove a transgene insertion at the 40D locus [46])
y w hsFLP; yki-venus His2Av-mRFP / +; FRT82B RFP-nls / FRT82B wts^{X1}
FRT19A sd^{47M} */ FRT19A Ubi-RFP-nls hsFLP; yki-venus His2Av-mRFP / +*
Sd-GFP; His2Av-mRFP / +
y w hsFLP; mastermind-EGFP / +; FRT82B RFP-nls / FRT82B wts^{X1}
NFAT-GFP; His2Av-mRFP/+
UAS-YFP / +; pannier-Gal4 UAS-His-RFP

Generation of the Yki-venus strain

The *yki-venus* strain was generated by CRISPR/Cas9-mediated targeted transgene integration [47, 48]. The gene encoding Venus fluorescent protein was inserted immediately in front of the stop codon of the *yki* gene so that Yki-Venus was translated as a C-terminal fusion protein. The donor vector carried approximately 1kb homology arms on either side of a knock-in cassette comprising genes encoding Venus and 3xP3-RFP [49] flanked by loxP sites. The gRNA expression vector included a 20-bp protospacer sequence, which was designed to include the Yki stop codon. The donor and gRNA vectors were co-injected into fertilized eggs laid by nos-Cas9 flies [50]. Transformants were selected by eye-specific red fluorescence of the 3xP3-RFP transgene, which was subsequently removed by crossing to hs-Cre.

Immunofluorescence

D. melanogaster larval eye and wing imaginal discs were dissected from third instar larvae, fixed in 4% paraformaldehyde (Proscitech), permeabilised in 0.3% Triton X-100 and stained with antibodies specific for Yki, GFP or CD2. DAPI was used to stain nuclei.

Immunoblotting

D. melanogaster wing imaginal discs were dissected from third instar larvae, lysed in protein loading buffer, subjected to SDS-PAGE and transferred to PVDF (Millipore). Membranes were immunoblotted with antibodies specific for Yki and Tubulin.

In vivo imaging of *D. melanogaster* pupae

For imaging of *D. melanogaster* pupae, pre-pupae of the appropriate genotype that had yet to undergo head eversion were selected from crosses and placed in to Petri dishes at 25°C to continue development. The pre-pupae were checked every four hours, and those that had undergone head eversion during that time were selected as being the appropriate age for imaging. Thus pupae were imaged from two hours after head eversion ± two hours. Head eversion occurs around 12 hours after white pre-pupa formation and is followed by a burst of mitoses in the pupal notum [18]. This developmental time-point provides an ideal setting to observe many epithelial cells undergoing mitosis in a relatively non-crowded epithelium. Pupae were mounted ventral side down on a piece of double sided Sellotape placed on a standard glass slide largely as in [18, 51]. The anterior dorsal two thirds of the pupal case was peeled back using Dumont no. 5 forceps. A ring of Vaseline was created around the tape using a 5ml syringe and a small piece of moist Whatman paper was placed within this ring to generate a humid atmosphere. A coverslip with a small drop of water was rested on the Vaseline ring such that the water created an interface between the pupa and the coverslip. Pupae were then imaged on an Olympus FVMPE-RS Multiphoton microscope using an XLPlan N 25 × 1.05NA water dipping objective at 20°C ± 1°C. Excitation lasers were InSight or MaiTai DeepSee multiphoton lasers. The InSight was tuned to 1120nm for RFP excitation. The MaiTai was tuned to 960nm for Venus and 920nm for GFP excitation. Laser lines were combined with an LCDM670-1050. Excitation and emission wavelengths were separated using a FV30-NDM760. Emission was separated by an FV30-SDM570. Wavelengths longer than 570nm (His-RFP signal) were deflected to a FV30-FOCy5 filter, consisting of a 650nm dichroic and 575-645nm filter and on to a PMT detector. Emission wavelengths shorter than 570nm (GFP and Venus) passed through either an FV30-FVG filter (for Venus) consisting of a 485nm dichroic and 495-540 filter, or an FV30-FGR filter (for GFP), consisting of a 570nm dichroic and 575-645 filter. GFP and Venus emission was detected using a GaAsP detector.

Quantification of time-lapse analysis of Yki-Venus

Images were acquired in the .oir format and opened using the Olympus viewer plugin for FIJI [43]. Background subtraction was carried out on each channel by subtracting the average intensity of an ROI drawn in a region with no objects. For the purposes of cell tracking, a median filter of radius 2 pixels was applied to the His-RFP channel, but for later intensity analysis, unfiltered data was used. Individual cell chromatin was tracked using the His-RFP channel using the 'semi-automatic' tracking function of the TrackMate plugin for FIJI [44]. Tracks were analyzed and incorrect tracking events were manually corrected. TrackMate tracks one daughter cell following mitosis, so untracked daughters were tracked and linked to the parent by a branching event. Spot radius was set to 5μm and time-lapse crops of individual cells were exported and saved as .tiff files using the 'Extract track stack' function of TrackMate. Due to movement of chromatin in the z imaging plane, this resulted in a 2D + time image series for each cell in which the middle slice of the total chromatin had been selected at each time-point. These images were then opened with Icy [45]. An ellipse ROI was drawn around the His-RFP signal in the first frame and the 'Active Contour' function of Icy was used to track the chromatin through subsequent frames, generating an area ROI at each time-point corresponding to the chromatin area, as marked by His-RFP. Errors in segmentation, such as incorporation of abutting chromatin in to the ROI were corrected manually. This ensured high quality, high confidence tracks of chromatin in all cases. Intensity measurements of Yki-Venus and His-RFP channels were extracted for all cells tracked in a video using a custom batch Icy protocol and the 'ROI statistics' function. Data were then analyzed and graphs generated using custom MATLAB (Mathworks) scripts, which synchronized all tracks *in silico* to the point of daughter chromatin separation during anaphase.

Ex vivo culture of wing imaginal discs

Third instar wandering larvae were cleaned in PBS, followed by 70% ethanol and rinsed in PBS. Larvae were dissected in culture media using Dumont no. 5 forceps by inverting the anterior half of the larvae. 1ml of culture media was composed of 855μl Schneiders Insect media (with 0.4% penicillin/streptomycin), 125μl insulin (10mg/ml stock) and 20μl FBS. Media was used within one day. The wing imaginal discs were carefully removed by grasping the trachea to avoid damaging the discs. The discs were then transferred to a coverslip using a pipette in a drop of fresh media. A fine ring of Vaseline was deposited around the culture media using a P200 pipette tip and an oxygen permeable membrane was placed on top to seal the media. The coverslip was then attached to an aluminum slide with a cut out using double sided tape and imaged using the same methods as pupae. Alternatively, wing discs were cultured in a perfusion chamber as for LMB experiments. Cultured discs were imaged within four hours of dissection.

Treatment of imaginal discs with leptomycin B

Wing imaginal discs were dissected from third instar larvae as for normal imaging experiments and then transferred in a drop of imaging media to a perfusion chamber (Grace Bio-Labs CoverWell GBL622503), which was then sealed with a coverslip. Imaging was carried out through the coverslip using the same methods as pupae. Pre-LMB treatment time-points were collected. The imaging chamber was then removed from the stage and the media replaced with LMB imaging media (containing 33nM LMB) by pipetting through the perfusion ports with a P200 pipette. The wing disc was gently and thoroughly pipetted up and down to ensure complete mixing with LMB media. The imaging chamber was then returned to the stage, and imaging was resumed four minutes after LMB media was added.

Quantification of nuclear accumulation rates

For LMB treatment of wing imaginal discs, at each time-point, and for each wing domain or genotype, at least 30 nuclei were manually outlined using a uniform circular ROI based on the His-RFP or His-RFP plus RFP-nls signal. Intensity values for each channel were background subtracted by measuring the signal intensity in an ROI containing no objects. Yki-Venus intensity was measured in each ROI and normalized to the RFP signal (except for sd^{47M} mosaic experiments, see below), and the mean nuclear Yki intensity was then calculated for each time-point and genotype/wing domain. Pre LMB values were averaged from the two pre-LMB time-points to generate a t = 0 value. For wts^{X1} mosaic wing discs, Yki-Venus intensity was further normalized to t = 0 due to the discrepancy in the RFP channel caused by the absence of RFP-nls in the wts^{X1} mutant tissue. Data were plotted and fitted using MATLAB to a mono-exponential function:

$$f(t) = a\left(1 - e^{-kt}\right) + c,$$

where a is the amplitude of the change in Yki-Venus intensity, k is the effective rate of import of Yki-Venus and c is the intensity-axis intercept. For LMB-treated sd^{47M} mosaic wing imaginal discs, to enable direct comparison of absolute Yki-Venus nuclear intensity between mutant and wild-type tissue (which have different nuclear RFP signal), no normalization was carried out. For wts^{X1} and sd^{47M} mosaic wing discs, clones were between 72 and 80 hours old and were induced with 1 hour heat shock at 37°C.

Fluorescence loss in photobleaching

Pupae were mounted and imaged as above. Prometaphase cells were identified by visible condensation of chromatin, marked by His-RFP. A field of 95 pixels square with a pixel size of 0.255μm was imaged for all experiments. Five time-points were collected of both the His-RFP and Yki-Venus or Sd-GFP signals before photobleaching. For photobleaching, a 5 × 5 pixel square region of the cytoplasm was repeatedly bleached and the Yki-Venus or Sd-GFP signal in a 95 pixel square field was subsequently imaged at an interval of 0.42 s for 280 time-points (around 2 minutes). After completion of the experiment, a post bleaching series of five frames of both His-RFP and Yki-Venus or Sd-GFP was collected to ensure that the chromatin had not drifted during the experiment. Data were excluded if the bleaching region encroached on the chromatin area or if the chromatin drifted out of the analysis ROI. Intensity values were analyzed at each time-point and FLIP curves were generated using the following equation from [21]. ROI_{nb} is the non-bleached ROI (experimental chromatin), ROI_{bg} is the background intensity. For Sd-GFP experiments, ROI_{bg} was a background ROI drawn in a region of the image that contained no chromatin, such that background measurements were taken at each time-point. This was not possible for Yki-Venus experiments due to the cytoplasmic localization of Yki-Venus, so a single background ROI was measured in a region outside the pupa and this was used for all time-points. ROI_n is an ROI drawn on neighboring cells to normalize for general bleaching during acquisition, and *pbROI* are average values from the corresponding ROIs from the first five pre-bleach frames, except for $pbROI_{bg}$ for Yki-Venus, as noted above.

$$\frac{\left(ROI_{nb} - ROI_{bg}\right)/\left(ROI_{n} - ROI_{bg}\right)}{\left(pbROI_{nb} - pbROI_{bg}\right)/\left(pbROI_{n} - pbROI_{bg}\right)}$$

Quantification of mitotic Yki-Venus

Quantification of Yki-Venus in wild-type and sd^{47M} tissue was performed from multiple mitotic events in a single pupa. Clones were induced by heat shocking larvae for 1 hour at 37°C approximately 75 hours before imaging. Wild-type and sd^{47M} mutant regions of the tissue were identified due to being homozygous or null for RFP-nls respectively. In addition to RFP-nls, cells also contained a His-RFP signal but wild-type cells were conspicuous due to the distribution of RFP-nls throughout the entire cell after nuclear envelope breakdown at prometaphase. Prior to measurement, background signal subtraction from the Yki-Venus channel was performed by subtracting the average intensity of an ROI drawn in a region outside of the pupal tissue. For prometaphase, metaphase and anaphase cells, ROIs were drawn around the His-RFP signal in the wild-type and sd^{47M} cells, and the average Yki-Venus intensity of each ROI was measured. Cells were classified as prometaphase, metaphase or anaphase prior to analysis by chromatin architecture. Prometaphase cells display visible condensation of chromatin, metaphase cells display fully compacted chromatin aligning on the metaphase plate, and anaphase cells are distinguishable following chromatin separation as chromatin moves toward the cell poles. Each data point represents an individual cell, except in the case of anaphase chromosomes, where each data point represents a separate segregating genome. Statistical analyses were unpaired t tests, performed in GraphPad Prism 7.

QUANTIFICATION AND STATISTICAL ANALYSIS

Statistical analysis was carried out using GraphPad Prism 7 or MATLAB. Details of statistical tests can be found in figure legends. Significance was defined as $p < 0.05$. No methods were used to carry out randomization or sample size estimation.